

Article

Warm Rolled Temperature Effect on Microstructure and Mechanical Properties of 18Mn/40Si2CrMo Multilayer Composite Steel

Bo Yang¹, Zhuoyu Li¹, Kuanyuan Fan¹, Baoxi Liu^{1,2,*}, Wenxing Yu^{3,*} and Fuxing Yin^{1,2,4,*} ¹ School of Materials Science and Engineering, Hebei University of Technology, Tianjin 300130, China² Tianjin Key Laboratory of Materials Laminating Fabrication and Interfacial Controlling Technology, Research Institute for Energy Equipment Materials, Tianjin 300000, China³ School of Mechanical Engineering, Hebei University of Technology, Tianjin 300130, China⁴ Institute of New Materials, Guangdong Academy of Sciences, Guangzhou 510651, China

* Correspondence: liubaoxiliubo@126.com (B.L.); yuwenxing128323@163.com (W.Y.); yinfuxing@hebut.edu.cn (F.Y.); Tel.: +86-156-2003-1851 (B.L.)

Abstract: In order to obtain a good strength-plastic/toughness match relationship, 18Mn/40Si2CrMo multilayer composite steels were successfully fabricated by a vacuum hot rolling and warm rolling process in this paper. The effects of different warm rolling temperatures (400–600 °C) on the microstructure and mechanical properties of the multilayer composite steel were systematically investigated. The result shows that the warm rolling process reduces thickness of the interfacial diffusion layer, which improves the interfacial bonding strength of multilayer composite steel. With the increase of warm rolling temperature, the total elongation (TEL) increases but ultimate tensile strength (UTS) decreases. The multilayer composite steel with a warm temperature of 500 °C achieves the balance of strength and plastic of which the UTS and TEL are 1.7 GPa and 12.5%, respectively. This is due to the high work-hardening ability of deformation twins of the 18Mn layer and the precipitates nanoscale carbides of the 40Si2CrMo layer to obscure the dislocation movement.

Keywords: multilayer composite steel; warm rolling; delamination; tensile properties

Citation: Yang, B.; Li, Z.; Fan, K.; Liu, B.; Yu, W.; Yin, F. Warm Rolled Temperature Effect on Microstructure and Mechanical Properties of 18Mn/40Si2CrMo Multilayer Composite Steel. *Crystals* **2022**, *12*, 1652. <https://doi.org/10.3390/cryst12111652>

Academic Editor: José L. García

Received: 17 October 2022

Accepted: 9 November 2022

Published: 17 November 2022

Publisher's Note: MDPI stays neutral with regard to jurisdictional claims in published maps and institutional affiliations.



Copyright: © 2022 by the authors. Licensee MDPI, Basel, Switzerland. This article is an open access article distributed under the terms and conditions of the Creative Commons Attribution (CC BY) license (<https://creativecommons.org/licenses/by/4.0/>).

1. Introduction

In the last few decades, with the improvement of global science and technology, in some major engineering areas, the higher requirement is put forward for the properties of metal materials, for example, it has high-strength and high-plasticity [1–3]. However, strength and plasticity are usually an inverted relationship, so it is a difficult assignment to achieve both high-strength and high-plasticity.

Recently, multilayer structure offers a novel idea. It refers to the composite of two or more materials by stacking and rolling, can inherit the properties of both materials [4–8]. Herein, metal multilayer materials with heterogeneous layers and bimetallic interfaces have received the attention of many researchers [9–13]. By laminating and rolling different metals, a variety of new materials can be designed to cope with a complex and harsh usage environment. In general, multilayer composite steel usually consists of soft and hard phases, during the deformation process, the stress and strain is redistributed in soft and hard layers, which gives the multilayer composite steel plate excellent mechanical properties; this makes the multilayer composite steel sheet have superior mechanical properties.

Multilayer metal composites have a long history. More than a thousand years ago, the Damascuses used repeated folding to make sharp knives. The knife has a pattern resembling water waves, and its microstructure is a layered material formed by the superposition of laminated ferrite and carburized body [14,15]. Its high strength and high toughness are caused by the carburizing layer and the ferritic layer, respectively. Liu et al. [16] successfully produced multilayer SUS304/Cr17 steels with laminate/network interface by

hot rolling and found that annealing treatment can induce alloy element diffusion and enhance interface bonding. Koseki et al. [17] reported that multilayer steel can achieve a good match between strength-elongation and good plastic formability compared with single steel. Wang et al. [18] achieved both strengthening and toughening by hot rolling stainless steel composite plates with mechanical properties, exhibiting an excellent ultimate strength of 543 MPa and fracture elongation of 52%.

In previous studies, most of the research on multilayer materials is limited to hot rolling experiments, but the strength of hot rolling is lower and the performance is poorer, and there is less research in the field of warm rolling. Compared with hot rolling, warm rolling can significantly improve mechanical properties, however, the effect of warm rolling temperatures on the performance of 18Mn/40Si2CrMo multilayer steel is not clear. Herein, 18Mn/40Si2CrMo multilayer composite steel was manufactured by vacuum hot rolling. Subsequently, the effect of different warm rolling temperatures on the interface morphology and element diffusion of multilayer composite steel plate was studied and the evolution of microstructure and toughening mechanism were systematically investigated. It provides a theoretical and experimental basis for the preparation of metal multilayer composite structures, fracture and toughening mechanisms.

2. Materials and Methods

18Mn and 40Si2CrMo were prepared by the vacuum melting method. Subsequently, the fabrication process of multilayer composite steel was as follows: firstly, 18Mn steel and 40Si2CrMo steel sheets with a standard thickness of 0.5 mm were taken as the initiation into the metal plate, and their chemical compositions are shown in Table 1. To remove oxide layers and impurities on the surface, sandpaper was used and cleaned with acetone, respectively, to obtain a clean metal surface, which facilitates the improvement of interfacial bond strength between the constituent layers. Secondly, stack 18Mn steel and 40Si2CrMo steel in an alternate A-B-A-B-A . . . arrangement in an unsealed carbon steel box, a total of 100 layers, as shown in Figure 1a. Thirdly, the carbon steel box is sealed by tungsten inert gas (TIG) welding and then a round hole with a diameter of 5 mm is drilled on the surface of the billet box, which is connected with a carbon steel pipe by welding. After the vacuum degree of the billet is reduced to 2.0×10^{-2} Pa by a triplex diffusion pump, the carbon steel pipe was pressed through hydraulic pliers. Finally, the billet was heated at 1200 °C, soaked for 60 min and then rapidly hot rolled (HR) with a reduction of 92% (HR-92), as shown in Figure 1b,c. Subsequently, the hot-rolled multilayer steels were warm rolled (WR) with five rolling temperatures of 400 °C (W-400), 450 °C (W-450), 500 °C (W-500), 550 °C (W-550), 600 °C (W-600), respectively, the total rolling reduction ratio is 95.2%. The diameter of working roll is 350 mm, the circumferential rate is 50 rpm, the strain rate of each hot rolling pass is 0.2, and the strain rate of each warm rolling pass is 0.1. In order to avoid excessive temperature reduction, the furnace is heated for 10 min for each two rolling passes.

Table 1. The chemical composition of raw 18Mn and 40Si2CrMo [wt.%].

Element	C	Mn	Al	Si	Cr	Mo	Fe
18Mn	0.62	17.48	1.46	≤0.1	≤0.1	≤0.05	80.19
40Si2CrMo	0.4	0.2	0.022	2.0	1.0	1.01	95.368

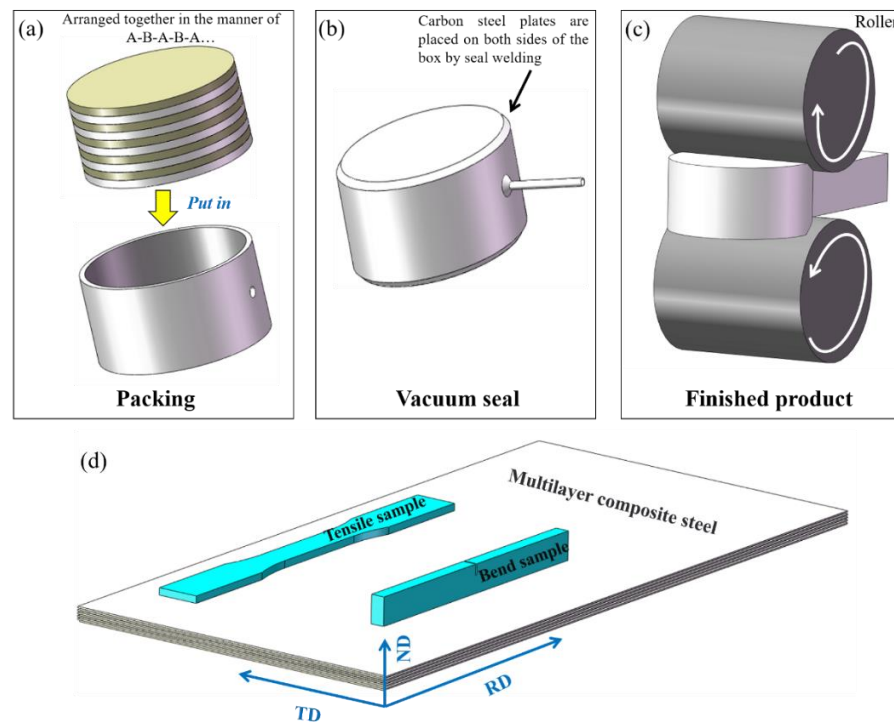


Figure 1. Schematic diagram of (a–c) fabrication process and (d) the tensile and bending samples of multilayer steels.

JSM-7100F scanning electron microscope (SEM), and its electron backscattered diffraction (EBSD) technique, Tecnai G2 F30 S-TWIN transmission electron microscopy (TEM), JXA-8530F electron probe microanalyzer (EPMA) were used to analyze interface bonding, element distribution, and microstructure evolution. Smartlab 9 KW X-ray diffraction (XRD) was used to analyze phase structure and dislocation density. HMV-G-XY-S microhardness tester was used to display the work-hardening behavior of the warm-rolled multilayer steel with different rolling temperatures. The AGS-50kNX universal testing machine was used to measure the tensile and bending properties of multilayer steels; the sample size for testing is shown in Figure 1d; five samples of each state were tested. The strain rate of tensile test was 1mm/min, and a YYJ-10/10-L electron extensometer was used to measure the elongation. The Vickers' hardness (HMV-G-FA) was estimated with HV0.2 and hold pressure for 15 s.

3. Results

3.1. Microstructure

Figure 2 shows the EBSD analysis of the hot-rolled multilayer composite steel (HR-92). As shown in Figure 2a, the 18Mn layer has a large grain size and forms a small portion of twins, while the 40Si2CrMo layer has a smaller grain size and the average grain size is $20 \pm 5 \mu\text{m}$ and $4 \pm 2 \mu\text{m}$, respectively. As shown in Figure 2b, the green areas are an 18Mn layer, which is face centered cubic (fcc) structure. The yellow areas are the 40Si2CrMo layer, which is body centered cubic (bcc) structure.

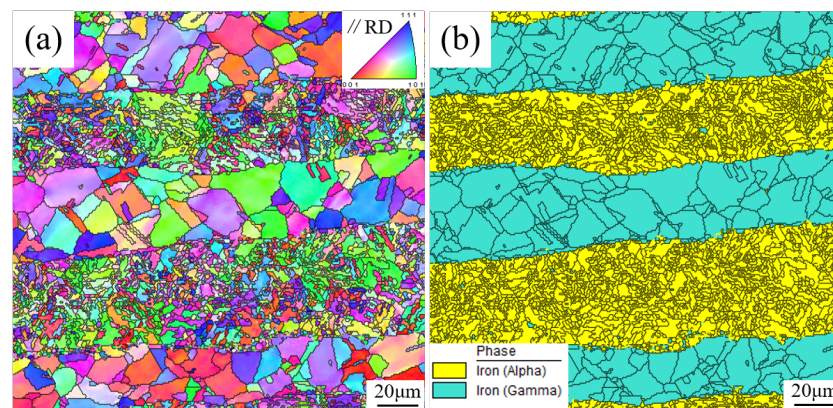


Figure 2. EBSD diagram for the hot-rolled sample: (a) Inverse pole figure; (b) phase figure and corresponding grain boundaries.

Figure 3 shows the EPMA surface scanning maps of multilayer 18Mn/40Si2CrMo steel. As can be seen from the figure, when the warm rolling temperatures are low, the interface shape is curved and local necking was found at lower temperatures (400–450 °C), because of different hardening rates of 18Mn and 40Si2CrMo leading to unstable behavior [19]. As the warm rolling temperature increases, the interface between the multilayer composite steel becomes flat, so the plastic deformation capacity can be improved by increasing the warm rolling temperatures.

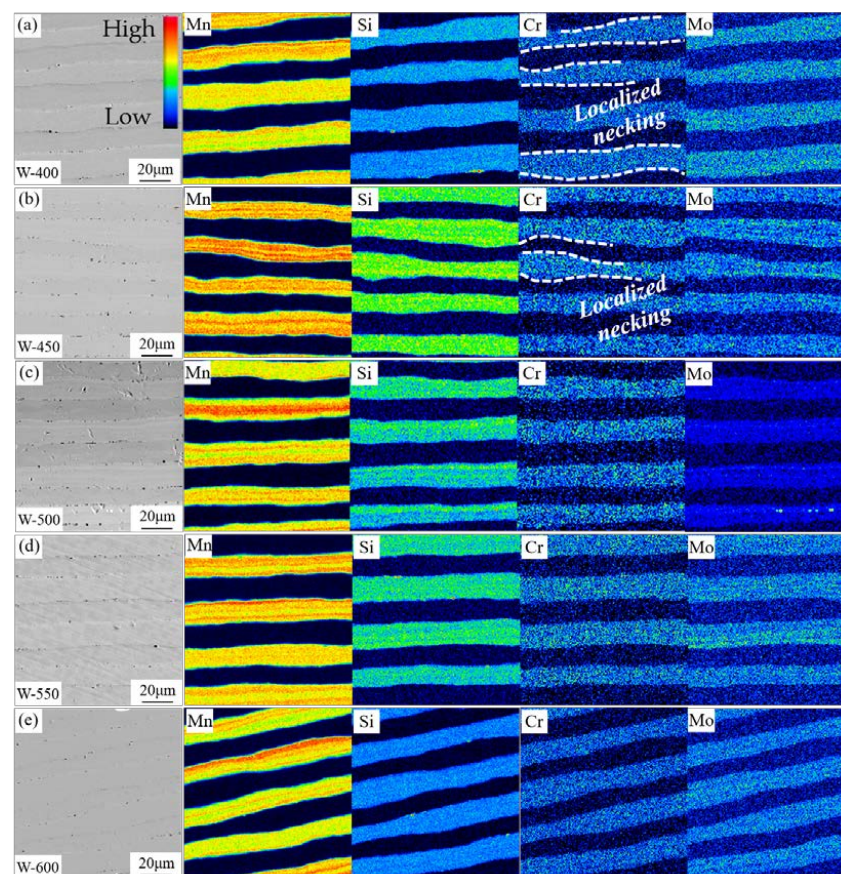


Figure 3. Elemental distribution of multi-layer composite steel at different rolling temperatures: (a) 400 °C; (b) 450 °C; (c) 500 °C; (d) 550 °C; (e) 600 °C.

Figure 4 shows the Mn, Si, Cr and Mo elemental distributions near the interface of the multilayer composite steel. According to Arrhenius equation [20]:

$$D = D_0 e^{\left(-\frac{Q}{RT}\right)} \quad (1)$$

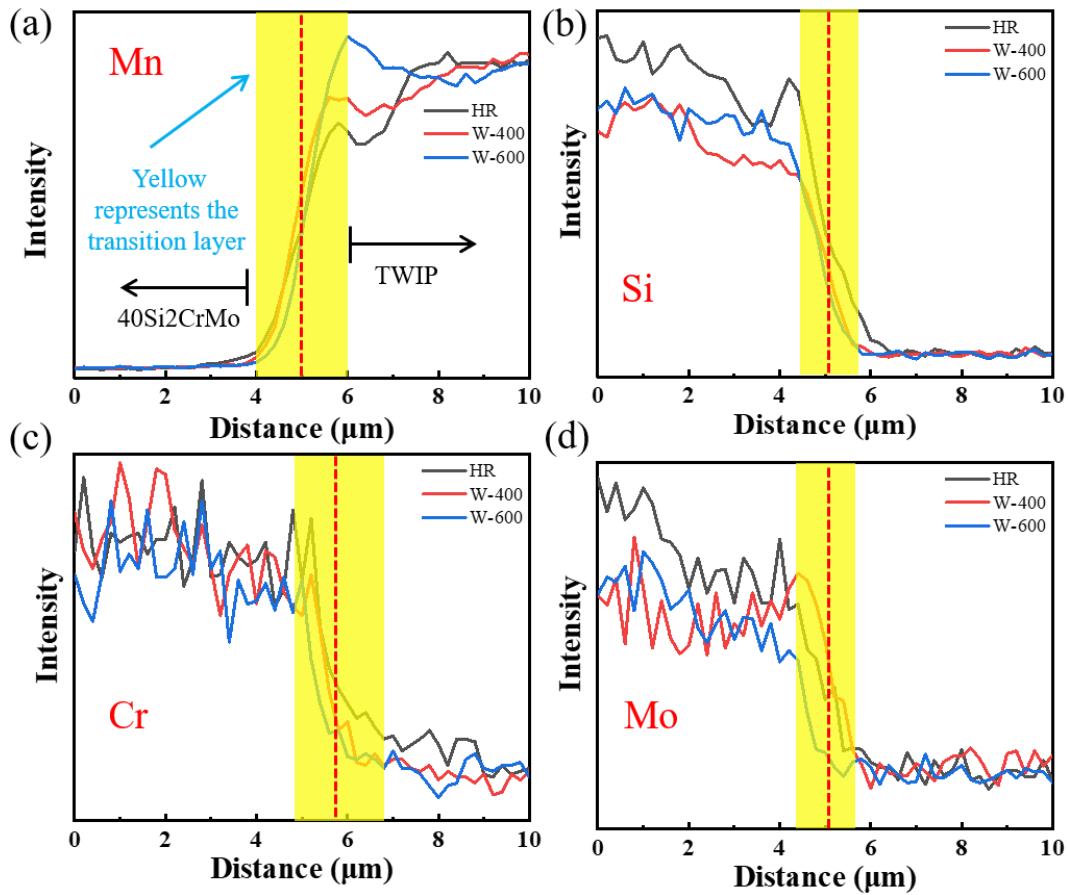


Figure 4. Elemental diffusion distances at the interface for different elements of the multilayer composite steel: (a) Mn element; (b) Si element; (c) Cr element; (d) Mo element.

D_0 is the diffusion constant, Q is the activation energy per mole of an atom, R is the gas constant, and T is thermodynamic temperature. Diffusion distance (X) is related to diffusion coefficient (D) and diffusion time (t),

$$X = 2\sqrt{Dt} \quad (2)$$

So, the diffusion coefficient is proportional to temperature, diffusion distance is proportional to the diffusion coefficient, and diffusion time.

$$D_{Mn} = 1.49 \times 10^{-4} e^{-\frac{66.4}{RT}} \quad (3)$$

$$D_{Cr} = 1.8 \times 10^4 e^{-\frac{97}{RT}} \quad (4)$$

$$D_{Mo} = 6.84 \times 10^{-2} e^{-\frac{59}{RT}} \quad (5)$$

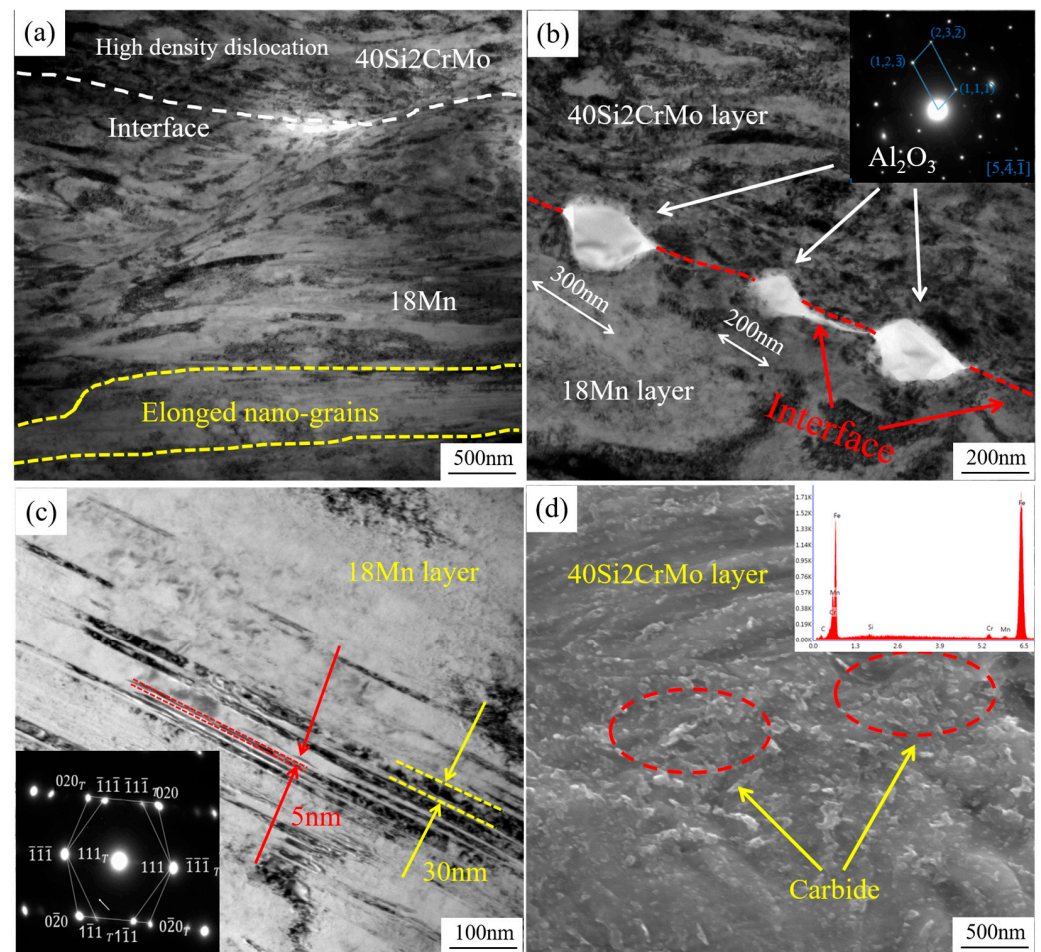
$$D_{Si} = 7 \times 10^{-6} e^{-\frac{243}{RT}} \quad (6)$$

The calculation results are shown in Table 2. In the same temperature range, $D_{Cr} > D_{Mn} > D_{Mo} > D_{Si}$, the diffusion driving force caused by concentration difference is small, and mutual diffusion will occur in the rolling process [17].

Table 2. Interfacial element diffusion distances of 18Mn/40Si2CrMo multilayer composite steel with different warm rolling temperatures.

Distance (μm)	HR-92	W-400	W-450	W-500	W-550	W-600
Mn	4.4	2.1	2.4	2.5	2.5	2.5
Si	2.8	2.2	1.9	2.1	1.8	2.6
Cr	4.4	2.4	2.6	2.6	2.6	3
Mo	3.2	1.6	2	1.8	2.2	2.4

Figure 5 shows the TEM and SEM microstructure of the W-500 sample. 18Mn layer and 40Si2CrMo layer produce strain incompatibility at the interface, resulting in a wavy interface. As rolling changes the state of strain, the 18Mn layer expands more than the 40Si2CrMo layer in the rolling direction, resulting in shear stresses at the interface and local shear bands, as shown in Figure 5a. Al_2O_3 are formed at the interface with a diameter between 200–300 nm, and the interfacial oxide can improve the interfacial bonding strength [21], Figure 5b. In the 18Mn layer, grain refinement, dislocation proliferation and twinning are evident, a large number of nanoscale grain boundaries and high-density dislocation are formed. As shown in Figure 5c, the width of the twins is mostly around 5–30 nm, nano-scale twin achieve reinforcement by the introducing high-density surfaces. In the 40Si2CrMo layer, the precipitated nanoscale carbides can pin the dislocation motion, thus improving the performance.

**Figure 5.** TEM and SEM images of 18Mn/40Si2CrMo multilayer composite steel plate at 500 °C: (a,b) interface; (c) the 18Mn layer; (d) the SEM image of 40Si2CrMo layer.

3.2. Tensile Properties and Hardness

Figure 6 shows the hardness distributions of multilayer steels with different warm rolling temperatures, compared with the HR-92, the hardness of the warm-rolled plate will be greatly improved. Li et al. [22] found that warm rolling deformation can significantly increase the dislocation density of austenitic steel, the free carbon atoms interact with high-density dislocations, and then dynamic strain aging occurs in the 18Mn layer, which improves the hardness. On the other hand, the formation of deformation twins in the 18Mn layer will further hinder the movement of dislocations and accelerate the plugging of dislocations. The dislocation density in the 40Si2CrMo layer increases as the warm rolling temperature decreases, and the further precipitation of fine carburized particles will also play a “pegging role” in the movement of dislocations, triggering the process hardening phenomenon. As the temperature rises, the hardness value gradually decreases, and the difference between the two layers decreases significantly, which increases the ratio of movable dislocation to immovable dislocation so that the hardness decreases [23].

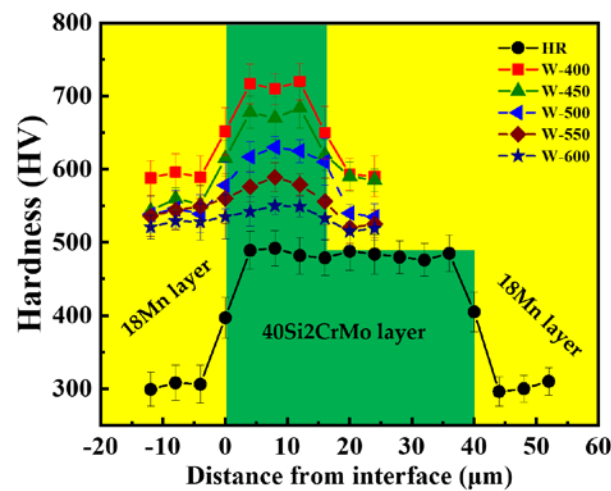


Figure 6. Hardness distribution of adjacent layers in composite steel.

Figure 7 shows the engineering stress–strain curves of multilayer composite steel with different warm rolling temperatures; the tensile properties are listed in Table 3. It is found that warm rolling can improve the yield strength (YS) and ultimate tensile strength (UTS) of HR-92. With the decrease of warm rolling temperature, the YS and TS increase continuously, while the total elongation (TEL) after fracture decreases; when the rolling temperature drops to 400 °C, the tensile strength is close to 2 GPa, but the elongation is too low to meet the requirements of most products. In conclusion, good comprehensive mechanical properties can be obtained at the temperature of 450–550 °C.

Table 3. Tensile properties of 18Mn/40Si2CrMo multilayer composite steel with different warm rolling temperatures.

Sample	UTS (MPa)	YS (MPa)	TEL (%)
HR	1028	1226	25.3
W-400	1879	1978	4.6
W-450	1760	1859	10.5
W-500	1670	1780	12.2
W-550	1496	1625	12.4
W-600	1340	1515	12.8

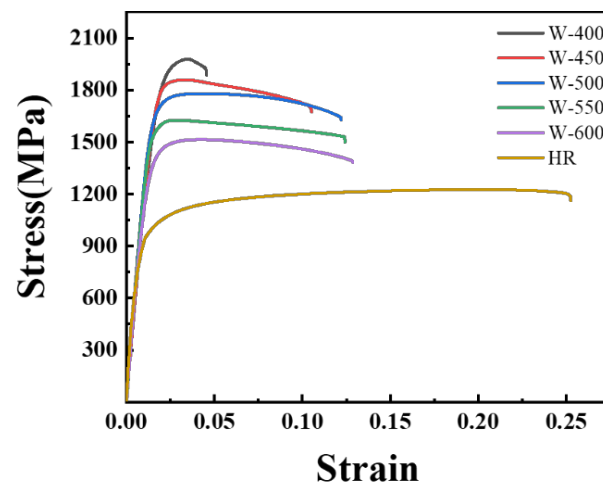


Figure 7. Engineering stress–strain curve of multilayer composite steel.

Figure 8 shows the normal fracture morphologies of multilayer 18Mn/40Si2CrMo sheets of steel with different warm rolling temperatures, the black box is enlarged below. All of them show obvious interfacial delamination, which indicates the increased plastic deformation capacity. Meanwhile, the fracture morphologies show dimples of two different sizes, with the increase of warm rolling temperature, the width of the transition layer at the interface increases gradually, this could be caused by the diffusion of elements at the interface [16]. The dimples of the 18Mn steel layer are large and deep, and the number is increasing, showing that the 18Mn layer has better plastic deformation ability than the 40Si2CrMo layer.

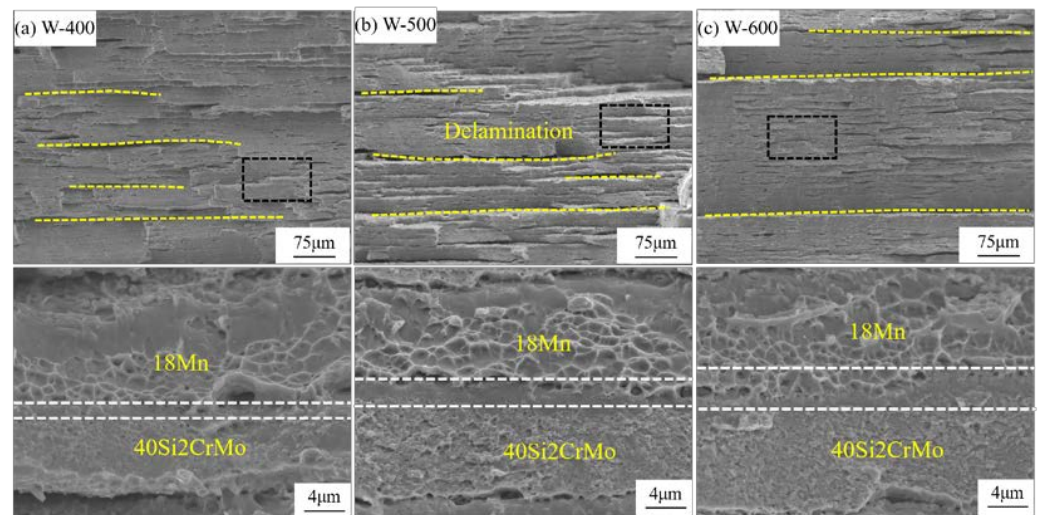


Figure 8. Tensile fracture morphology of multilayer composite steel at different temperatures: (a) 400 °C; (b) 500 °C; (c) 600 °C.

In a previous study, Kimura et al. [24,25] prepared ultrafine elongated grain structure (UFEG) with layered distribution by tempforming technology. Multilayer composite steel has many similarities with the fracture mode of UFEG, when subjected to bending loads; significant delamination occurs because of the anisotropic UFEG structure. The local strain state of the crack tip can be changed from triaxial to uniaxial by delamination, causing the cracks blunting. In addition, the delamination causes the crack growth rate to slow down and change from a dynamic state to a low-rate state, resulting in plastic deformation, thus showing high toughness.

During bending deformation, the position close to the indenter is not easy to form cracks due to compressive stress, while the position far away from the indenter is prone to

crack initiation and propagation due to tensile stress. The crack perpendicular to the layer direction is easy to deflect at interface. As shown in Figure 9, with the increase in warm rolling temperature, the number of crack propagation retarded and deflected increased significantly, the crack propagation path is increased, as shown by the red arrow, the crack propagation energy is consumed, and the anti-crack propagation ability of multilayer composite steel is improved [26,27]. Figure 10 shows the bending stress–strain curves of multilayer composite steel with different warm rolling temperatures, with the decrease of warm rolling temperature, the growth rate of initial bending stress becomes faster, and the yield point increases, so does the bending strength.

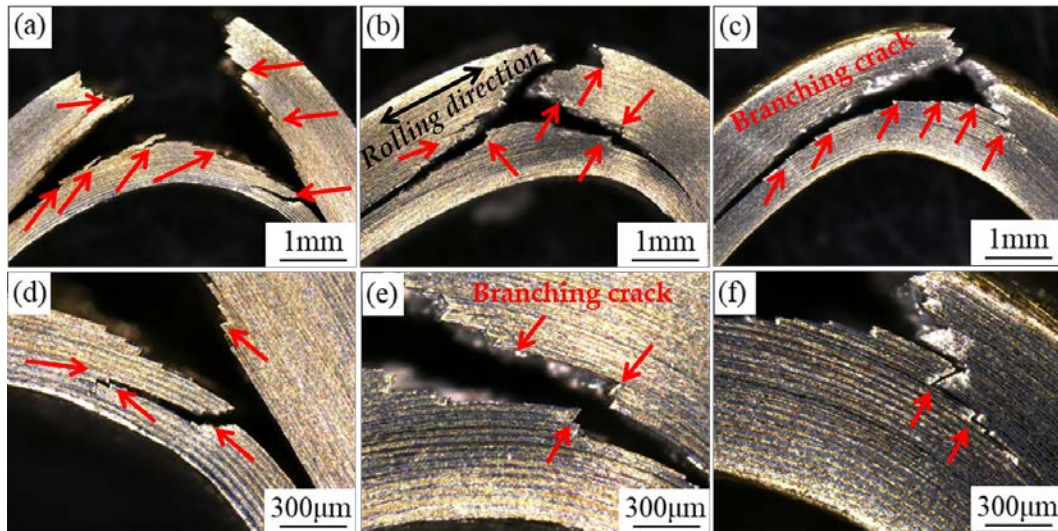


Figure 9. Bending fracture morphology of multilayer composite steel at different rolling temperatures, (d–f) is the enlarged view of (a–c): (a) 400 °C; (b) 500 °C; (c) 600 °C.

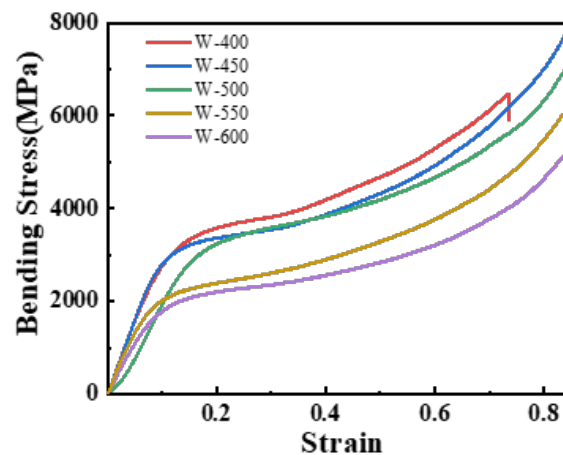


Figure 10. Bending stress–strain curve of multilayer composite steel.

4. Discussion

In this study, it was found that the warm rolling process can obtain multilayer composite steel with excellent performance. Compared with cold rolling, warm rolling can significantly reduce the microstructure damage and optimize the microstructure; the reinforcement mechanisms for each group element layer are discussed further below.

Twin boundary as a special coherent grain boundary not only hinders the movement of dislocation to improve the strength of the 18Mn layer but also serves as a dislocation slip surface to absorb and store dislocation and to improve the plastic deformation ability. Curtze et al. [28] found that there are two main deformation mechanisms in 18Mn steel,

twinning strengthening and dislocation slip, which are related to the magnitude of Stacking fault energy (SFE). 18Mn steel is mainly deformed by twinning when the SFE is between 20–40 mJ/m². When the SFE is greater than 45 mJ/m², dislocation slip is the main strengthening mechanism. The calculated SFE value of 18Mn at room temperature is 26.80 mJ/m², so the deformation strengthening mechanism of the 18Mn layer is mainly twinning.

As shown in Figure 5c, a large number of nano-scale twins appear in the 18Mn layer, which will hinder the movement of the dislocations and change the movable dislocation into immobile dislocation [29], strain hardening behavior is produced and the strength is increased. In addition, the stress concentration and applied shear stress on the twin interface will increase with the increase of the number of dislocations plug, and the number of pluggable dislocations within the twin decreases with the thinning of the twinning layer. When the thickness of the lamina is too low to be pluggable, an extremely high applied stress is required to force a single dislocation across the twin boundary [30,31].

There are many diffusively distributed carbide particles in the 40Si2CrMo layer, approximately 30–80 nm in diameter, as shown in Figure 5d. Fine nano-carbides can pin dislocations, produce work hardening and improve strength. The interaction between nano precipitates and dislocations can be divided into two mechanisms. First, when the sliding resistance of the precipitated phase is less than the maximum reaction force of dislocation slip motion, the nano-precipitated phase can be regarded as deformable particles and thus be cut by dislocation. Second, if the resistance of relative dislocation precipitated is greater than or equal to the reaction force of dislocation slip motion, the nanoparticles become immovable particles, resulting in the strengthening of the dislocation bypass mechanism [32]. In fact, the strengthening mechanism of carbide is mainly determined by the ratio of the carbide diameter *R* to the Burgers vector *b* [33]. If *R/b* < 15, it is mainly dislocation cutting mechanism, and if *R/b* ≥ 15, it is mainly dislocation bypassing mechanism. 40Si2CrMo has *R/b* = 12.5 < 15, so the main strengthening mechanism is dislocation cutting mechanism.

Figure 11 shows the X-ray Diffraction patterns of multilayer composite steel with different warm rolling temperatures. Compared with the diffraction peak of hot-rolled multilayer composite steel plate, no new phase is generated after warm rolling, and the (200) γ diffraction peak disappears, (111) γ diffraction peak and (110) α diffraction peak decrease in intensity. To determine the dislocation densities for multilayer steel with different process parameters, the Scherrer formula can be used to calculate [34], the dislocation density is related to the average microcrystalline size and microstrain, which microcrystalline size and microstrain can be estimated according to the Scherrer formula and Williamson–Hall formula, respectively [20,35], the relevant calculation results are shown in Table 4.

$$D = \frac{k\gamma}{B\cos\theta} \quad (7)$$

$$\frac{B\cos\theta}{\lambda} = \frac{2\langle\epsilon_{50}^2\rangle\sin\theta}{\lambda} + \frac{K}{d'} \quad (8)$$

D is the average microcrystal size, *K* is Schell factor, *K* = 1, γ is the wavelength of the X-ray, γ = 0.154056 nm. *B* is full width at half maximum, θ is Bragg angle. ϵ_{50}^2 is microstrain, λ is the wavelength of the K_{α} , λ = 0.15418 nm, *d'* is average grain size. The calculation formula of dislocation density is shown in Formula (9).

$$\rho = \frac{3(2\pi)^{\frac{1}{2}}}{Db} \langle\epsilon_{50}^2\rangle \quad (9)$$

b is the Burgers vector, *b* = 2.5 × 10^{−7} mm. According to Formula (4), the contribution value of dislocation to material strengthening in 18Mn layer and 40Si2CrMo layer was estimated, respectively.

$$\sigma_{\text{dis}} = \alpha M G b \rho^{\frac{1}{2}} \quad (10)$$

σ_{dis} is dislocation density contribution, α is constant, $\alpha = 2$. $M = 2.9$ [36], G is shear modulus, $G = 7.1 \times 10^4$ MPa.

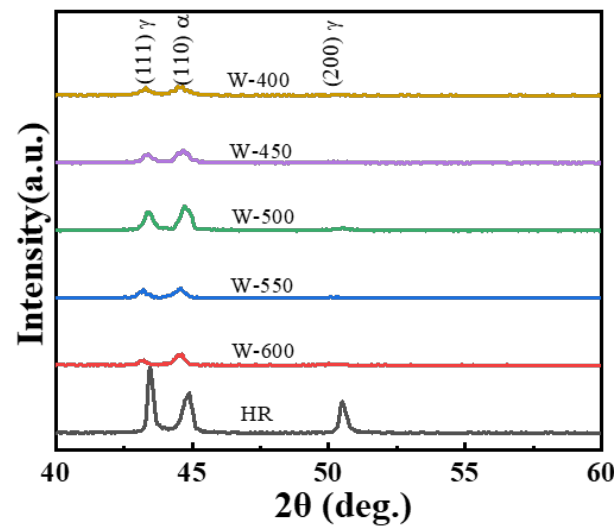


Figure 11. XRD patterns of 18Mn/40Si2CrMo multilayer composite steel plates with different rolling warm temperatures.

Table 4. The full width at half maximum, dislocation densities, and dislocation enhancement value for 18Mn/40Si2CrMo multilayer composite steel with different parameters.

18Mn/40Si2CrMo		The Full Half Maximum (B)	Dislocation Density (mm^{-2})	Dislocation Enhancement Value (MPa)
Hot rolling	18Mn	0.209	9.953×10^6	324.8
	40Si2CrMo	0.325	1.492×10^7	397.7
W-400	18Mn	0.366	3.051×10^7	566.8
	40Si2CrMo	0.468	4.781×10^7	712.3
W-450	18Mn	0.359	2.934×10^7	557.6
	40Si2CrMo	0.430	4.035×10^7	654.0
W-500	18Mn	0.351	2.808×10^7	545.5
	40Si2CrMo	0.396	3.425×10^7	602.5
W-550	18Mn	0.311	2.203×10^7	483.2
	40Si2CrMo	0.382	3.190×10^7	581.5
W-600	18Mn	0.277	1.746×10^7	430.2
	40Si2CrMo	0.358	2.797×10^7	544.5

5. Conclusions

1. The multilayer composite steel in the hot rolled state has good deformation coordination and the interface transitions to wavy as the warm rolling proceeds. Local necking occurs to varying degrees between both layers, which is due to the difference in hardening rates and flow stresses between 18Mn and 40Si2CrMo, resulting in shear stresses at the interface;
2. The diffusion distance of Mn, Si, Cr, and Mo at the interface all increase with the increase of warm rolling temperature, which is mainly due to the increase of diffusion coefficient caused by the increase of temperature;
3. As the warm rolling temperature decreases, the YS and UTS increase, TEL decreases. When the warm rolling temperature is 500 °C, the YS of the sample reaches 1670 MPa, YS reaches 1780 MPa, and the TEL is 12.2%, which is an excellent strength-plasticity combination;

4. In the bending process, lower warm rolling temperature leads to premature failure with a low number of deflection cracks, while with a higher warm rolling temperature due to good interfacial bonding, multiple cracks are passivated; there are numerous deflection cracks formed, and continuous crack deflection and delamination can absorb a large amount of energy, thus enhancing the bending resistance.

Author Contributions: Conceptualization, B.L.; methodology, W.Y.; software, Z.L.; validation, B.Y.; formal analysis, B.Y.; investigation, B.Y. and B.L.; resources, B.Y.; data curation, K.F.; writing—original draft preparation, B.Y.; writing—review and editing, B.Y. and B.L.; visualization, K.F.; supervision, F.Y.; project administration, F.Y.; funding acquisition, F.Y. All authors have read and agreed to the published version of the manuscript.

Funding: The authors gratefully acknowledge financial support from the Natural Science Foundation of Hebei, China (No. E2020202124, E2021202075), the foundation strengthening program (No: 2019-JCJQ-142-00), the Key-Area R&D Program of Guangdong Province (2020B010134000), and the Guangdong Academy of Science (2021GDASYL-20210102002).

Institutional Review Board Statement: Not applicable.

Informed Consent Statement: Not applicable.

Data Availability Statement: Not applicable.

Conflicts of Interest: We declare that we have no financial and personal relationships with other people or organizations that can inappropriately influence our work, and there are no professional or other personal interests of any nature or kind in any product, service, and/or company that could be construed as influencing the position presented in the review of the manuscript, entitled by “Warm Rolled Temperature Effect on Microstructure and Mechanical Properties of 18Mn/40Si2CrMo Multilayer Composite Steel”.

References

1. Zhu, Z.; He, Y.; Zhang, X.; Liu, H.; Li, X. Effect of interface oxides on shear properties of hot-rolled stainless steel clad plate. *Mater. Sci. Eng. A* **2016**, *669*, 344–349. [[CrossRef](#)]
2. Chen, L.; Yang, Z.; Jha, B.; Xia, G.; Stevenson, J.W. Clad metals, roll bonding and their applications for SOFC interconnects. *J. Power Sources* **2005**, *152*, 40–45. [[CrossRef](#)]
3. Gholami, M.D.; Davoodi, B.; Hashemi, R. Study of forming limit curves and mechanical properties of three-layered brass (CuZn10)/ low carbon steel (St14) /brass (CuZn10) composite considering the effect of annealing temperature. *J. Mater. Res. Technol.* **2022**, *18*, 4672–4682. [[CrossRef](#)]
4. Foadian, F.; Soltanieh, M.; Adeli, M.; Etminanbakhsh, M. The Kinetics of TiAl₃ Formation in Explosively Welded Ti-Al Multilayers During Heat Treatment. *Metall. Mater. Trans. B* **2016**, *47*, 2931–2937. [[CrossRef](#)]
5. Basak, S.; Mondal, M.; Gao, K.; Hong, S.-T.; Anaman, S.Y.; Cho, H.-H. Friction stir butt-welding of roll clad aluminum thin sheets: Effect of microstructural and texture changes on mechanical properties. *Mater. Sci. Eng. A* **2022**, *832*, 142490. [[CrossRef](#)]
6. Hosseini, M.; Pardis, N.; Manesh, H.D.; Abbasi, M.; Kim, D.-I. Structural characteristics of Cu/Ti bimetal composite produced by accumulative roll-bonding (ARB). *Mater. Des.* **2017**, *113*, 128–136. [[CrossRef](#)]
7. Tan, H.F.; Zhang, B.; Luo, X.M.; Sun, X.D.; Zhang, G.P. Strain rate dependent tensile plasticity of ultrafine-grained Cu/Ni laminated composites. *Mater. Sci. Eng. A* **2014**, *609*, 318–322. [[CrossRef](#)]
8. Kim, H.Y.; Chung, D.S.; Hong, S.H. Reaction synthesis and microstructures of NiAl/Ni micro-laminated composites. *Mater. Sci. Eng. A* **2005**, *396*, 376–384. [[CrossRef](#)]
9. Romero, A.; Rodríguez, G.P.; Marjaliza, E. Processing of intermetallic laminates by Self-Propagating High-Temperature Synthesis initiated with concentrated solar energy. *J. Alloys Compd.* **2021**, *891*, 161876. [[CrossRef](#)]
10. Ding, H.; Cui, X.; Wang, Z.; Zhao, T.; Wang, Y.; Zhang, Y.; Chen, H.; Huang, L.; Geng, L.; Chen, J. A new strategy for fabrication of unique heterostructured titanium laminates and visually tracking their synchronous evolution of strain partitions versus microstructure. *J. Mater. Sci. Technol.* **2022**, *107*, 70–81. [[CrossRef](#)]
11. Inoue, J.; Nambu, S.; Ishimoto, Y.; Koseki, T. Fracture elongation of brittle/ductile multilayered steel composites with a strong interface. *Scripta Mater.* **2008**, *59*, 1055–1058. [[CrossRef](#)]
12. Nambu, S.; Michiuchi, M.; Inoue, J.; Koseki, T. Effect of interfacial bonding strength on tensile ductility of multilayered steel composites. *Compos. Sci. Technol.* **2009**, *69*, 1936–1941. [[CrossRef](#)]
13. Cao, W.; Zhang, M.; Huang, C.; Xiao, S.; Dong, H.; Weng, Y. Ultrahigh Charpy impact toughness (~450J) achieved in high strength ferrite/martensite laminated steels. *Sci. Rep.* **2017**, *7*, 41459. [[CrossRef](#)] [[PubMed](#)]

14. Sherby, O.D.; Wadsworth, J. Ancient blacksmiths, the Iron Age, Damascus steels, and modern metallurgy. *J. Mater. Process. Technol.* **2001**, *117*, 347–353. [[CrossRef](#)]
15. Bruschi, S.; Cao, J.; Merklein, M.; Yanagimoto, J. Forming of metal-based composite parts. *CIRP Ann.* **2021**, *70*, 567–588. [[CrossRef](#)]
16. Liu, B.X.; An, Q.; Ge, Y.F.; Yin, F.X.; Zhang, B.Y.; Yu, W.X.; Ji, P.G.; Zhang, X.; Chen, C.X. Deformation Behavior and Strengthening Mechanisms of Multilayer SUS304/Cr17 Steels with Laminate/Network Interface. *Metall. Mater. Trans. A* **2020**, *51*, 3658–3673. [[CrossRef](#)]
17. Koseki, T.; Inoue, J.; Nambu, S. Development of Multilayer Steels for Improved Combinations of High Strength and High Ductility. *Mater. Trans.* **2014**, *55*, 227–237. [[CrossRef](#)]
18. Wang, S.; Liu, B.X.; Chen, C.X.; Feng, J.H.; Yin, F.X. Microstructure, mechanical properties and interface bonding mechanism of hot-rolled stainless steel clad plates at different rolling reduction ratios. *J. Alloys Compd.* **2018**, *766*, 517–526. [[CrossRef](#)]
19. Zhang, B.Y.; Liu, B.X.; He, J.N.; Ji, P.G.; Zhang, X.; Fang, W.; Feng, J.H.; Hu, X.L.; Yin, F.X. A new route to fabricate multilayer steel with multiscale hierarchical structure. *Mater. Charact.* **2020**, *169*, 110606. [[CrossRef](#)]
20. He, H.; Liu, Y.; Yin, J.; Wang, X.; Lin, X.; Zhang, S. Introducing effective temperature into Arrhenius equation with Meyer-Neldel rule for describing both Arrhenius and non-Arrhenius dependent drain current of amorphous InGaZnO TFTs. *Solid State Electron.* **2021**, *181–182*, 108011. [[CrossRef](#)]
21. Zhang, X.; Fan, X.; Yan, C.; Li, H.; Zhu, Y.; Li, X.; Yu, L. Interfacial Microstructure and Properties of Carbon Fiber Composites Modified with Graphene Oxide. *ACS. Appl. Mater. Inter.* **2012**, *4*, 1543–1552. [[CrossRef](#)] [[PubMed](#)]
22. Li, J.; Jiang, F.; Li, Y.; Zhang, M.; Chen, C.; Yang, Z.; Zhang, F. Effect of warm-rolling on the strength and ductility of multilayered composite steel. *Mater. Sci. Eng. A* **2022**, *841*, 143043. [[CrossRef](#)]
23. Busby, J.T.; Hash, M.C.; Was, G.S. The relationship between hardness and yield stress in irradiated austenitic and ferritic steels. *J. Nucl. Mater.* **2005**, *336*, 267–278. [[CrossRef](#)]
24. Kimura, Y.; Inoue, T.; Yin, F.; Tsuzaki, K. Inverse temperature dependence of toughness in an ultrafine grain-structure steel. *Science* **2008**, *320*, 1057–1060. [[CrossRef](#)] [[PubMed](#)]
25. Kimura, Y.; Inoue, T. Mechanical Property of Ultrafine Elongated Grain Structure Steel Processed by Warm Tempforming and Its Application to Ultra-High-Strength Bolt. *ISIJ Int.* **2020**, *60*, 1108–1126. [[CrossRef](#)]
26. Inoue, T.; Kimura, Y. Effect of Delamination and Grain Refinement on Fracture Energy of Ultrafine-Grained Steel Determined Using an Instrumented Charpy Impact Test. *Materials* **2022**, *15*, 837. [[CrossRef](#)] [[PubMed](#)]
27. Inoue, T.; Qiu, H.; Ueji, R.; Kimura, Y. Ductile-to-Brittle Transition and Brittle Fracture Stress of Ultrafine-Grained Low-Carbon Steel. *Materials* **2021**, *14*, 1634. [[CrossRef](#)]
28. Curtze, S.; Kuokkala, V.T. Dependence of tensile deformation behavior of TWIP steels on stacking fault energy, temperature and strain rate. *Acta Mater.* **2010**, *58*, 5129–5141. [[CrossRef](#)]
29. Bönisch, M.; Wu, Y.; Sehitoglu, H. Hardening by slip-twin and twin-twin interactions in FeMnNiCoCr. *Acta Mater.* **2018**, *153*, 391–403. [[CrossRef](#)]
30. Shen, Y.F.; Lu, L.; Lu, Q.H.; Jin, Z.H.; Lu, K. Tensile properties of copper with nano-scale twins. *Scripta Mater.* **2005**, *52*, 989–994. [[CrossRef](#)]
31. Kulkarni, Y.; Asaro, R.; Farkas, D. Are nanotwinned structures in fcc metals optimal for strength, ductility and grain stability? *Scripta Mater.* **2009**, *60*, 532–535. [[CrossRef](#)]
32. Jiang, S.; Wang, H.; Wu, Y.; Liu, X.; Chen, H.; Yao, M.; Gault, B.; Ponge, D.; Raabe, D.; Hirata, A.; et al. Ultrastrong steel via minimal lattice misfit and high-density nanoprecipitation. *Nature* **2017**, *544*, 460–464. [[CrossRef](#)]
33. Pan, D.; Zhao, Y.; Xu, X.; Wang, Y.; Jiang, W.; Chong, X. A novel strengthening and toughening strategy for T250 maraging steel: Cluster-orientation governed higher strength-ductility combination induced by electropulsing. *Mater. Design.* **2019**, *169*, 107686. [[CrossRef](#)]
34. Kamikawa, N.; Sato, K.; Miyamoto, G.; Murayama, M.; Sekido, N.; Tsuzaki, K.; Furuhashi, T. Stress–strain behavior of ferrite and bainite with nano-precipitation in low carbon steels. *Acta Mater.* **2015**, *83*, 383–396. [[CrossRef](#)]
35. Williamson, G.K.; Hall, W.H. X-ray Line Broadening from Filed Aluminum and Wolfram. *Acta Mater.* **1953**, *1*, 22–31. [[CrossRef](#)]
36. Sauzay, M.; Fournier, B.; Mottot, M.; Pineau, A.; Monnet, I. Cyclic softening of martensitic steels at high temperature—Experiments and physically based modelling. *Mater. Sci. Eng. A* **2008**, *483–484*, 410–414. [[CrossRef](#)]